RESEARCH ARTICLE

Tannic Acid-mediated Multifunctional 3D Printed Composite Hydrogel for Osteochondral Regeneration

Lanlan Dong[1,†], Zhengzhe Han[2,†], Xiang Li[1]*

[1]School of Mechanical Engineering, Shanghai Jiao Tong University, Shanghai 200240, China
[2]Department of Orthopedic Surgery, Shanghai Institute of Microsurgery on Extremities, Shanghai Jiao Tong University Affiliated Sixth People's Hospital, Shanghai 200233, China
†*These authors contributed equally to this work*

Abstract: Hydrogels have become an attractive option for tissue repair. A novel multifunctional hydrogel was developed using a two-step method involving photopolymerization and tannic acid (TA) solution incubation. The mechanical properties of this hydrogel were enhanced by the multi-hydrogen bond interaction between the TA and N-acryloyl glycinamide/gelatin methacrylate (NAGA/GelMA). The compressive modulus was doubled. The compressive strengths of the hydrogel were 5.5 MPa. The swelling rate was reduced by a factor of three. The adhesion strength of the composite hydrogel reached 80 KPa. The TA-mediated NAGA/GelMA/Laponite composite hydrogel exhibited excellent anti-fatigue and anti-oxidation properties, as well as printability. *In vitro* experiments indicated that the TA-mediated hydrogel facilitated the proliferation of bone marrow mesenchymal stem cells and osteogenic and chondrogenic differentiation. The developed multifunctional composite hydrogel has great potential for osteochondral defect repair under osteoarthritis conditions.

Keywords: Multifunctional hydrogel; Tannic acid; Mechanical properties; Antioxidant; Biocompatibility

***Correspondence to:** Xiang Li, School of Mechanical Engineering, Shanghai Jiao Tong University, 800 Dongchuan Road, Shanghai 200240, China: xiangliwj@sjtu.edu.cn

Received: March 14, 2022; **Accepted:** April 20, 2022; **Published Online:** July 5, 2022

Citation: Dong L, Han Z, Li X, 2022. Tannic Acid-mediated Multifunctional 3D Printed Composite Hydrogel for Osteochondral Regeneration. *Int J Bioprint*, 8(3):587. http://doi.org/10.18063/ijb.v8i3.587

1. Introduction

Hydrogel contains a large number of three-dimensional (3D) polymer networks formed by physical or chemical crosslinking. Their advantages include an extracellular matrix-like environment, a polymer network with high water content, biological activity, and flexibility similar to tissues[1,2]. Hydrogels have attracted extensive attention in tissue engineering and regeneration medicine, with wound dressing, bone-guided regeneration membrane, cartilage regeneration, and conductive cardiopathy applications[3-6]. Most natural hydrogels such as alginate, silk fibroin, chitosan, collagen, and gelatin have relatively poor mechanical properties, which hinder their applications in tissue engineering. This is especially crucial for cartilage tissue, requiring high strength and endurance[7,8]. Therefore, there have been numerous attempts to develop a high-strength hydrogel[9-11]. A printable, stretchable, and tough hydrogel comparable to natural cartilage was developed by combining polyvinyl alcohol (PVA) and sodium alginate[12]. Composite hydrogels based on polyacrylamide with sodium alginate have been proved to possess excellent mechanical properties such as high strength, toughness, and stretchability[13]. However, some deficiencies, including multi-step polymerization schemes, time-consuming experimental procedures, and potential cytotoxicity, have restricted their further applications in tissue repair[14]. N-acryloyl glycinamide (NAGA), a photopolymerizable hydrogel, has become a hot research topic because of its excellent mechanical properties. Zhai *et al*.[15] prepared a composite hydrogel composed of NAGA and clay to repair skull defects. High-strength hydrogels also hold promise for osteochondral tissue repair.

In addition, a hydrogel used for osteochondral repair should meet the following requirements. Its mechanical properties should match those of natural cartilage[6]. It is essential that the hydrogel adheres to the surrounding

tissues during regeneration to prevent any treatment invalidation caused by the detachment of the two parts[16]. Under osteoarthritis conditions, hydrogels with antioxidant properties are indispensable[17]. These diseased conditions could produce excess reactive oxygen species and generate oxidative stress that damages the redox balance, which suppresses osteogenic differentiation[18,19]. Hence, for hydrogel applications in osteochondral repair, it is essential to obtain a synergistic effect involving good biocompatibility, high mechanical performance, excellent oxidation resistance, and adhesion to realize multifunctionality.

Tannic acid (TA) is a plant polyphenol with good anti-inflammatory, antibacterial, and antioxidant properties that have attracted widespread interest in biomedical applications[20]. Recent studies have demonstrated that TA combines with polyacrylamide or PVA to form a composite hydrogel with solid adhesion, toughness, and oxidation resistance[21-23]. However, because of the polymerization inhibition properties of TA, it is challenging to introduce TA directly into photoinitiated polymers. In addition, a hydrogel synthesized in one pot has submicrometer- or nano-sized networks, which obstruct the exchange of nutrients and oxygen. It drastically inhibits the proliferation and differentiation of cells[24]. 3D printing technology can solve this problem by precisely controlling the macropore structure within the hydrogel scaffold.[24,25]

Therefore, it was hypothesized that TA incubation could provide a simple and effective strategy for preparing multifunctional hydrogels. The TA, which contained many pyrogallol groups, was inserted into a covalent polymer consisting of gelatin methacrylate (GelMA) and NAGA. The copolymerization of GelMA and NAGA formed a leading network. By adding polyphenol compounds, multiple hydrogen bonds occurred between the phenolic hydroxyl group of TA, the carbonyl group, and the amino group of NAGA/GelMA. The two-step method prevented the polymerization inhibition effect of polyphenols. The hydrogel's morphology, chemical structure, swelling behavior, mechanical properties, and cell compatibility were characterized. The adhesion and oxidation resistance of the hydrogels were tested. Subsequently, the influence of clay and GelMA on the printability of the hydrogel was examined. In addition, the biocompatibility of the hydrogel and the potential of osteogenic and chondrogenic were evaluated.

2. Materials and methods

2.1. Materials

Gelatin (from porcine skin, Type A, powder, gel strength 240~270 Bloom) was purchased from Yeasen (Shanghai, China), methacrylic anhydride (MA), and 2-hydroxy-2-methyl-1-phenyl-1-propanone (IRGACURE 1173, 98%) were purchased from Sigma Aldrich (USA), Laponite XLG (LPN) was purchased from BYK (UK), NAGA was purchased from Zhengzhou Alfa Chemical Co., Ltd (Zhengzhou, China). TA and 1,1-diphenyl-2-picrylhydrazyl (DPPH) were purchased from Aladdin Co., Ltd (Shanghai, China). 2,2-azinobis (3-ethylbenzothiazoline -6-sulfonic acid mmonium salt) (ABTS), potassium persulfate ($K_2S_2O_8$), 2-Phenyl-4,4,5,5- tetramethylimidazoline-3-oxide-1-oxyl (PTIO), and borax were purchased from Beijing Innochem Science and Technology., Ltd (China).

2.2. GelMA synthesis

GelMA was synthesized following previous methods[26,27]. Briefly, 10 g gelatin was dissolved in 100 ml carbonate-bicarbonate buffer at 50°C under constant stirring. MA (2 ml) was slowly added to the above-mentioned solution. After reacting for 3 h, the pH of the solution was adjusted to neutral using hydrochloric acid or sodium hydroxide. GelMA was obtained after the resulting solution was dialyzed, filtered, and freeze-dried.

2.3. Preparation of composite hydrogel

A series of NAGA/GelMA/Laponite (denoted as NGL, where N, G, and L represent NAGA, GelMA, and LPN, respectively) composite hydrogels (**Table 1**) were prepared. First, deionized water (5 g), NAGA (3 g), and GelMA (1 g) were mixed and added to a 20 mL beaker under constant stirring for 30 min. Then, the photoinitiator Irgacure 1173 (100 μL) was added to the above solution. LPN (0.3 g) was then dispersed in 5 mL of deionized water. Subsequently, the NAGA/GelMA solution was mixed with the LPN suspension. After complete dissolution, the resulting solution was added into plastic molds (diameter 10 mm and thickness 5 mm) and exposed to an ultraviolet (UV) crosslinker (Chitang Co., Ltd., Shanghai, China, 16 W) for 40 min. The obtained NGL3 hydrogel was immersed in an aqueous solution with various amounts of TA (5 and 10 w/v %) for 24 h to obtain T5 and T10 hydrogels, respectively (the 1 w/v % borax was added at a specific time).

2.4. Physicochemical characterization of hydrogel

The microstructures of freeze-dried samples were analyzed by a field emission scanning electron microscope, Zeiss, Germany. Fourier transform infrared spectroscopy (FTIR, Nicolet iN10, Thermo Scientific, USA) was used to identify the chemical structure of the samples.

(1) Mechanical property

Compression testing of the hydrogel was performed using a Zwick Z050 in the press mode. In brief, a photocrosslinked hydrogel cylinder (6 mm in height and 10 mm in diameter; n = 3) was placed on the lower plate, and the speed was set at 1 mm/min. The

Table 1. Compositions and codes of different hydrogel.

NAGA (g)	GelMA (g)	LPN (g)	Water (mL)	1173 (μL)	TA	Brox	Code
3	1	0.3	10	100	–	–	NGL3
3	1	0.5	10	100	–	–	NGL5
3	1	0.3	10	100	(0.5 g) 10 ml	0.1g	T5
3	1	0.3	10	100	(1 g) 10 ml	0.1g	T10
3	1	0.3	10	100	(0.5 g) 10 ml	–	TA5
3	1	0.3	10	100	(1 g) 10 ml	–	TA10
3	1	0.3	10	100	(2 g) 10 ml	–	TA20
3	1	0.3	10	100	(3 g) 10 ml	–	TA30
3	1	0.3	10	100	(4 g) 10 ml	–	TA40
3	1	0.3	10	100	(5 g) 10 ml	–	TA50

compressive modulus was calculated from the slope of the stress–strain curve. The cyclic compressive tests were conducted using 15 loading-unloading cycles at a strain of 30% without intervals between consecutive cycles. The dissipated energy (Uhys) was quantified according to the area between the loading and unloading curves. The recovery rate of the hydrogels was calculated according to the following formula:

$$Recovery\,rate = \frac{U_{15}}{U_0} \times 100\%$$

where U_0 is the initial dissipated energy of the sample, and U_{15} is the energy dissipation after 15 cycles.

(2) Adhesive property

The adhesion strength was measured (n = 5) using a lap shear test of the hydrogel under air conditions, based on a previously reported method with minor modifications[28]. The hydrogel was applied to a piece of glass and sandwiched using another glass slide. The bonded area was fixed at 10 × 10 mm. The samples were incubated for 2 h at room temperature. The glass slides were pulled until they separated using a dynamic thermomechanical mechanical analyzer. The adhesion strength was calculated by dividing the maximum load by the bonded area. In addition, hydrogel was also applied between different materials. The substrates selected for the investigation included plastic, ceramics, rubber, leaves, metal, skin, and bone (The skin and bone were bought from the local supermarket).

(3) In vitro antioxidant activity

The antioxidant activity of the T5 hydrogel was measured by ABTS (2,2-azinobis-(3-ethylbenzthiazoline-6-sulfonic acid), DPPH (2,2-diphenyl-1-picrylhydrazyl) and PTIO (2-phenyl-4,4,5,5-tetramethylimidazoline-1-oxyl 3-oxide) assays using a previously reported method[29-31]. For the DPPH assay, a DPPH/ethanol (40 μg/mL) solution was prepared for the measurement. Then, the hydrogel (50 mg) was incubated in DPPH solution and allowed to react for 0.5 h in the dark. The absorbance at 517 nm was recorded using an UV-visible spectrophotometer (Thermo EV300, USA). An ABTS solution with an absorbance of 0.7 at 732 nm was prepared with a 7.4 mM ABTS stock solution and 2.6 mM $K_2S_2O_8$ aqueous solution. Then, 50 mg of the hydrogel sample was incubated in the ABTS solution at 25°C in the dark for 0.5 h. The absorbance at 734 nm of the prepared solution was measured using an UV-visible spectrophotometer assay. A PTIO solution was prepared with an absorbance of 0.2 – 0.6 at 557 nm. Then, 50 mg of the hydrogel sample was incubated in the PTIO solution at 25°C in the dark for 2 h. The absorbance at 557 nm of the prepared solution was measured using an UV-visible spectrophotometer assay. The free radical-scavenging rate was calculated using the following formula:

$$Inhibition\% = \frac{A_0 - A}{A_0} \times 100\%$$

where A_0 is the absorbance of the DPPH, ABTS, or PTIO solution, and A is the absorbance of the hydrogel mixed with the above solution. Each sample was analyzed in triplicate.

2.5. 3D-printing and rheological characterization of hydrogel

The prepared NGL hydrogel was printed by an extrusion 3D bioprinter in our laboratory (printing parameters: Inner diameter of needle: 400 μm; layer height: 300 μm; and strand spacing: 500 μm.) The printed samples were cross-linked under UV irradiation for 40 min. The viscoelastic property of each hydrogel (NAGA, NGL3, and NGL5) was evaluated using a rheometer at 25°C in a range of 0.1 – 1000 s^{-1} (Kinexus Ultra; Malvern, UK). The frequency

sweeps of the samples (0.1 – 100 Hz) were performed at room temperature in the obtained linear viscoelastic region. The storage modulus (G') and loss modulus (G") of the samples were measured in a frequency range of 0.1 – 100 Hz. The recovery properties were quantitatively characterized at room temperature using a rheometer. An alternate shear strain sweep test was performed at a frequency of 1 Hz to test the recovery ability of the hydrogel. The shear strain was switched successively from a minor strain of 1% (100 s) to a large strain of 100%, 200%, or 300% (100 s). After each phase of the test, the next stage began immediately without retention.

2.6. Biocompatibility and osteochondral activity of hydrogel

Bone marrow mesenchymal stem cells (BMSCs) were chosen to evaluate the biocompatibility of the hydrogel by cell counting kit-8 assays. The osteogenic differentiation on the hydrogels was evaluated by alizarin red staining (ARS), alkaline phosphatase (ALP) staining, and quantitative real-time polymerase chain reaction (qRT-PCR) assays. The chondrogenic differentiation on the hydrogels was evaluated by qRT-PCR assays. The details are available in Supplementary File.

2.7. Statistical analysis

Data were analyzed by one-way analysis of variance with Turkey's *post hoc* test (SPSS, version 17.0, USA) and expressed as the mean ± standard deviation. $P < 0.05$ was reported as significant for all statistical tests ($*P < 0.05$), and $P < 0.01$ was reported as highly significant for all statistical tests ($**P < 0.01$).

3. Results and discussion

3.1. Morphology, FTIR, and *in vitro* swelling of the hydrogel

Microstructural characterization revealed that the freeze-dried NAGA hydrogel exhibited a microfibrous structure (**Figure 1A**). This might have resulted from the strong intermolecular interactions of the hydrogen bonds. **Figure 1B and C** showed that the clay was intercalated into the NAGA/GelMA hydrogel[14]. As the clay content and tannin content increased, the gel network became denser (**Figure 1B-E**). In addition, as the TA concentration increased, the pore size of the TA-mediated hydrogel was obviously reduced, and the T10 sample possessed morphology similar to that of TA (**Figure 1E and F**). This might have been because the higher TA concentration improved the crosslink density by forming hydrogen bonds[30]. The macroscopic observations of NGL3, T5, and T10 hydrogel were presented in **Figure S1**.

As shown in **Figure 2A**, in the NGL3 spectrum, it was easy to observe the characteristic Si-O peak of LPN (1000 cm^{-1}), the characteristic N-H peak at 1558 cm^{-1} arose from NAGA, the characteristic peaks at 1658 cm^{-1} corresponding to C=O, -OH, and N-H stretching bands at 3300 cm^{-1} originated from GelMA and NAGA. The polymerization reaction caused the 1622 cm^{-1} band for NAGA (representing the characteristic peak of C=C) to disappear, indicating that the composite hydrogel was successfully formed after UV irradiation[32]. Compared with NGL, the TA-mediated hydrogel exhibited overlapping TA signals, indicating that the TA was incorporated into the NGL hydrogel network. The formation of broad bands at 3290 (-OH stretching vibration), and the movement of the -OH stretching vibration to a lower wavenumber in the T5 spectrum, indicated that a large number of hydrogen bonds were constructed between the TA and NGL[4].

The high swelling rate of the hydrogel could squeeze the surrounding tissues of the affected area, thereby affecting the repair of a defect. **Figure 2B** shows the swelling characteristics of four different hydrogels. Because the hydrophilic groups of the GelMA backbones were easily hydrated, the equilibrium swelling rates of the prepared hydrogels ranged from 600 to 900%. The TA-mediated hydrogel reached swelling equilibrium within 12 h. It has been previously shown that TA has a positive impact on the swelling properties of TA-mediated composite hydrogel, and the swelling mainly occurred within the first 4 h, which also confirmed the formation of hydrogen bonds in the TA-mediated hydrogel. As previously mentioned, the addition of TA produced a hydrogel with a higher crosslink density and smaller pore size, obstructing the diffusion of water into the hydrogel, which reduced the swelling ratio.

3.2. Mechanical properties of hydrogels

Ideal mechanical properties are essential for biomaterials because hydrogels need sufficient mechanical strength to withstand the squeezing of surrounding tissues. As shown in **Figure 3A**, the compressive modulus doubled. The compressive modulus reached 0.65 MPa for T5 (**Figure 3B** and **Table S1**), close to the compression modulus and compressive strength of human articular cartilage (0.4 – 0.8 MPa)[33]. There was no significant difference in the compressive modulus of NGL3 and NGL5 (**Figure 3B and C**). LPN by forming physical entanglement with NAGA/GelMA chains as well as themselves can disrupt the covalent network (established during NAGA/GelMA polymerization) and weaken the compressive modulus. At the same time, an increase in the concentration of nanoclay used as the "filler" increases the compression modulus. Therefore, balancing these two effects would result in no significant change in the compressive modulus[34]. However, when the TA content reached 10%, the compressive modulus of the material was significantly reduced, which might be

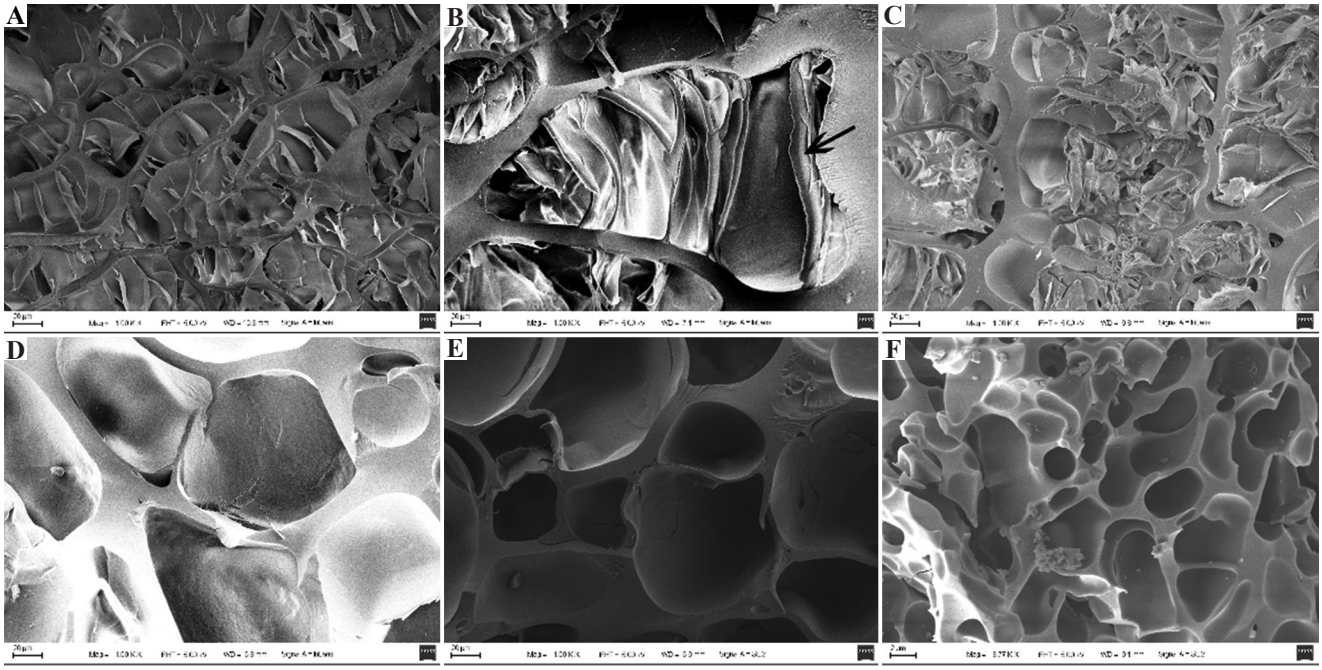

Figure 1. Scanning electron microscope images of composite hydrogels: (A) N-acryloyl glycinamide, (B) NGL3, (C) NGL5, (D) T5, (E) T10 (scale bar: 20 μm), and (F) tannic acid (scale bar: 2 μm).

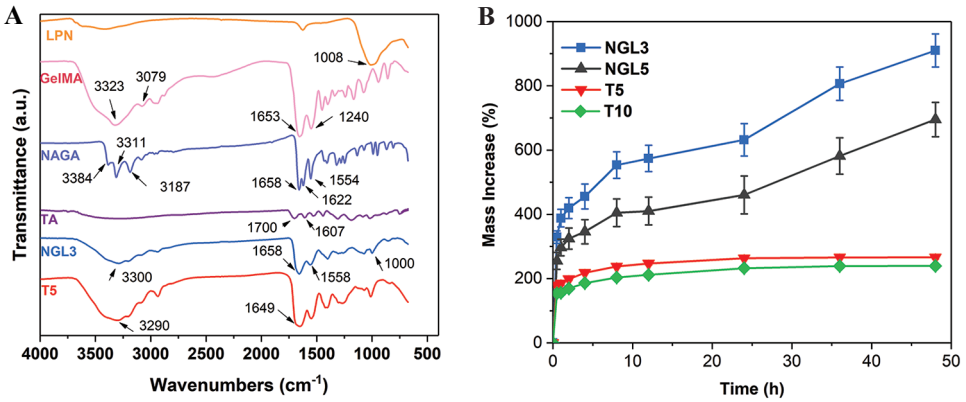

Figure 2. (A) FTIR spectra of pure LPN, GelMA, NAGA, TA, NGL3, and T5 composite hydrogel and (B) swelling behaviors of hydrogels.

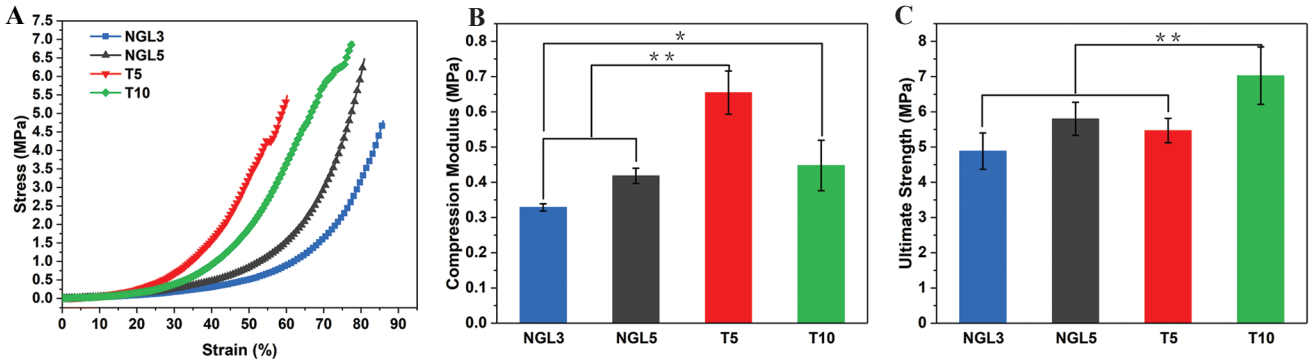

Figure 3. Mechanical evaluation of NGL3, NGL5, T5, and T10 hydrogels. (A) representative compressive strain–stress curves, (B) compressive modulus, and (C) compressive strength of different hydrogels.

attributed to the fragile polymer chains resulting from the high crosslinking density[35,36]. Therefore, the following fatigue tests were performed on the NGL3, NGL5, and T5 groups.

In practical applications, a biomaterial should possess sufficient fatigue resistance properties to maintain its mechanical strength and structural integrity. After 15 compressive test cycles at 30% strain, no fracture was observed, indicating that the hydrogel possessed good fatigue resistance (**Figure 4A-C**). When 30% strain was applied, the dynamic hydrogen bond tended to destroy the energy dissipation first to protect the covalent network of NAGA[10]. However, this inevitably destroyed the covalent bond network. As a result, a large hysteresis loop was observed in the first loading-unloading cycle. These unique properties would allow the hydrogels to be more widely used.

Figure 4D showed that the addition of clay increased hysteresis. The hysteresis could result in the energy absorbed during permanent deformation[34]. As shown in **Figure 4E**, the shape recovery rate of the NGL3 hydrogel after 15 cycles was 63%, while that of NGL5 was 43%. At the same time, in the T5 group under 30% strain, the shape recovery rate after 15 cycles was 57.9%, which could not fully reach the 100% recovery rate. This could be due to water loss during the loading process and the failure to absorb water over time. In short, the T5 group had the largest hysteresis loop area and the highest ultimate stress, which indicated that it possessed the largest storage modulus, consistent with the rheological data discussed later. As a result, it was proved that composite hydrogels with excellent mechanical properties could be synthesized under the synergistic effect of clay and TA treatment.

3.3. Adhesive property of the hydrogel

As shown in **Figure 5A**, increased TA content exhibited a positive impact on the bond strength, and the adhesive strength of the TA50 gel was as high as 80 KPa. Incorporating TA into the hydrogel could endow the TA hydrogel with excellent adhesion attributed to the catechol group[37]. Furthermore, borax was introduced into the TA solution under the assumption that the addition of borax would form a borate bond *in situ* and further enhance the adhesion ability. The lap shear test proved this assumption. The addition of 1% borax significantly improved the adhesive strength of the hydrogel. There was no significant difference between T5 (59.9 ± 3.5 KPa) and TA40 (56.9 ± 2.5 KPa).

The adhesion of the hydrogel to the surfaces of different materials was also evaluated. As shown in **Figure 5B**, the T5 hydrogel could adhere to various substrates, including plastic, rubber, ceramic, a leaf, glass, metal, skin, and bone. It is worth noting that the T5 hydrogel could also lift 500 g of weight. As shown in **Figure 5B-vii and viii**, the T5 hydrogel could easily lift a 100-g weight or lift a 48 g plastic bottle to the top, indicating that it possessed excellent underwater adhesion. Its superb toughness and self-adhesion would allow the T5 gel to be directly attached to irregular surfaces. As shown in **Figure 5B-ix**, the gel could adhere to the index finger and deform with the movement of joints. Therefore, the hydrogel exhibited good deformation adaptability.

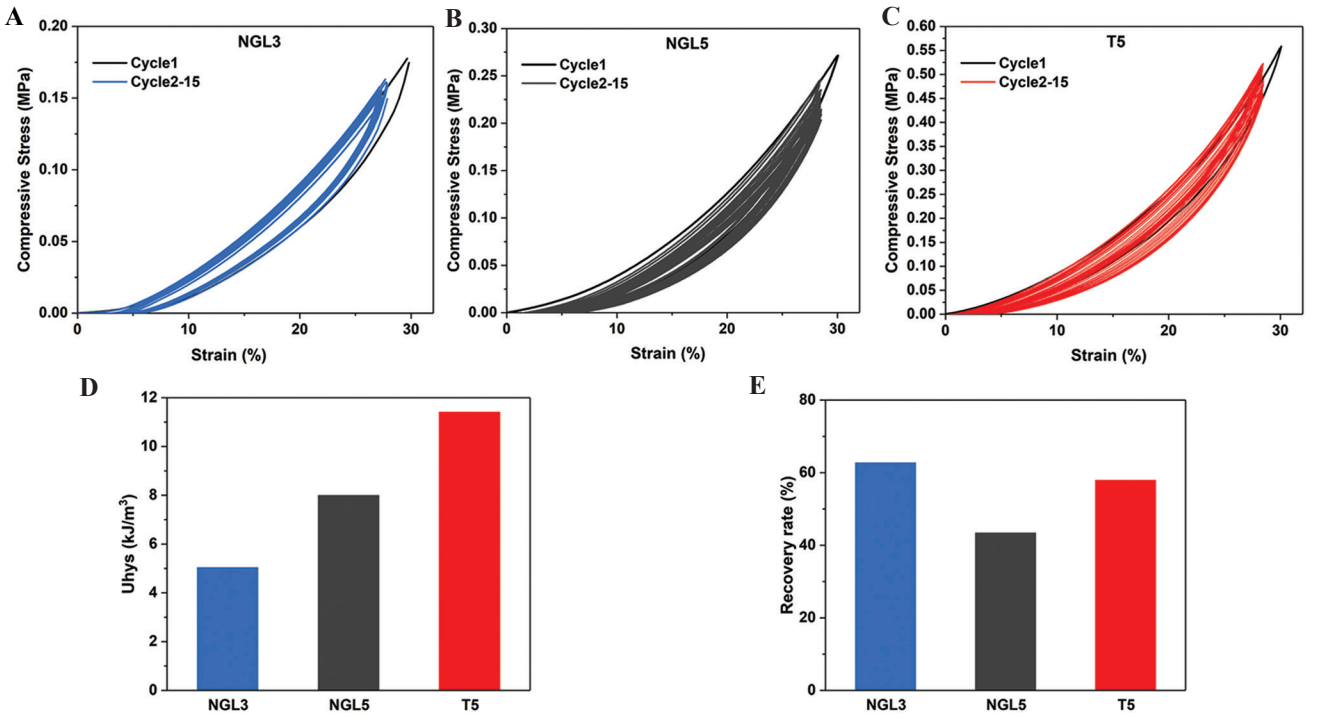

Figure 4. Compressive loading-unloading curves from the cyclic fatigue resistance tests of (A) NGL3, (B) NGL5, and (C) T5 hydrogel. (D) The calculated dissipated energy values and (E) toughness recovery rates of different hydrogels under 30% compressive strain.

The increase in the adhesion strength was attributed to the borate ester formed by borax and polyphenols. Consequently, when tested with various substrates, the T5 hydrogel exhibited universal adhesive properties and excellent adhesion to different underwater substrates, indicating its universal potential as an adhesive material for medical applications.

3.4. Antioxidant property of hydrogels

The ABTS, DPPH, and PTIO methods were used to evaluate the antioxidative efficiency of T5 hydrogel. As shown in **Figure 6A-C**, the ABTS, DPPH, and PTIO solutions were demonstrated in blue, purple, and blue-violet, respectively. When the T5 hydrogel was added to the solution, the absorbance sharply decreased, and all the original colors in the solution changed to light yellow. Because the PTIO method measures the transfer capacity of oxygen free radicals[38], it was confirmed that the antioxidant capacity of the hydrogel was concentration-dependent.

As shown in **Figure 6F**, a higher TA content led to a greater clearance rate for the sample. However, when the TA content exceeded 10%, the clearance rate was no significant difference between the T10 and TA powder

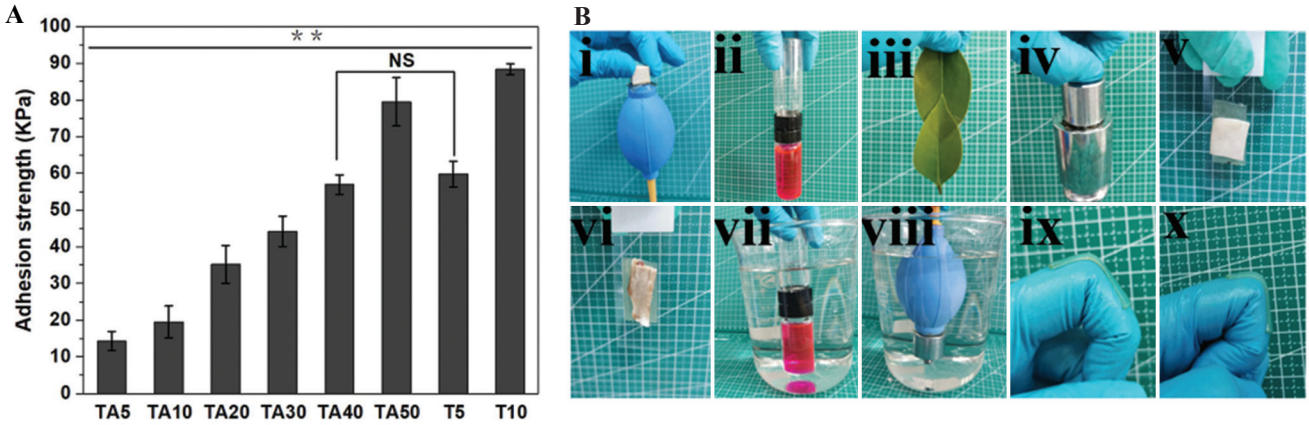

Figure 5. Adhesive properties of hydrogels. (A) The lap-shear adhesive strengths of different hydrogels on glass. (B) (i, ii, iii, iv, v, and vi) Various adherent surfaces, including rubber, ceramic, plastic, leaf, metal, skin, and bone. (vii, viii) Underwater adhesive behavior of T5 hydrogel with plastic and stainless-steel weight (100 g). (ix, x) Adhesion to finger and movement with joints.

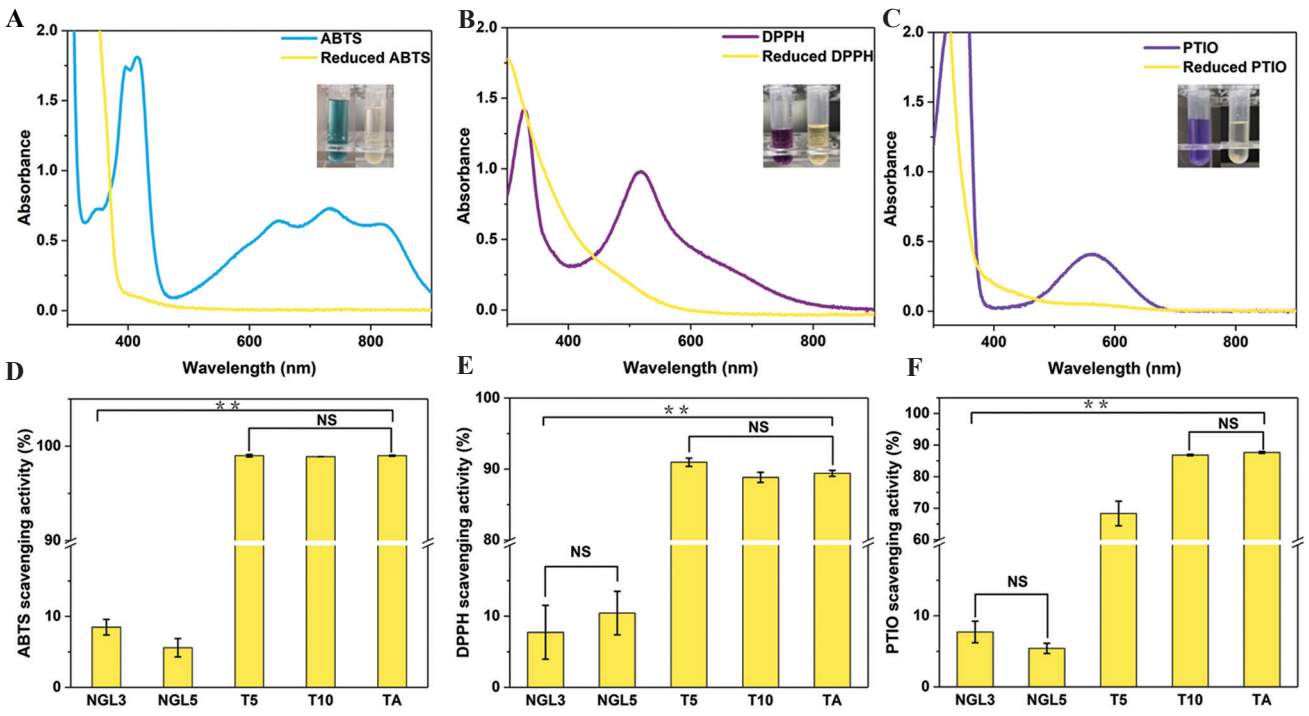

Figure 6. Absorbance changes of ABTS (A), DPPH (B), and PTIO (C) when exposed to T5 hydrogel. ABTS (D), DPPH (E), and PTIO (F) scavenging activities with different samples.

(**Figure 6D-F**). These results showed that the introduction of TA improved the antioxidant capacity of the hydrogel. The high hydroxyl group was the main factor explaining the high antioxidant activity of the TA[4]. Oxidative stress commonly occurs in patients with osteoarthritis. Thus, hydrogels with an antioxidant capacity have great potential to enhance osteogenesis[17].

3.5. 3D printing and rheological characterization of hydrogels

Before printing the scaffold, the viscosities of the NAGA and NGL inks were measured, which was a critical factor in determining the printability of these inks. When using extrusion-based 3D printing, a shear-thinning behavior for the ink is beneficial for the gel–sol conversion of the material. As shown in **Figure 7A**, as the shear rate increased, the viscosity of the NGL3 and NGL5 hydrogels rapidly decreased, showing the typical shear-thinning behavior. In addition, the viscosity of the pure NAGA ink did not change with the shear rate, indicating the behavior of a Newtonian fluid. The above results showed that the NGL3 and NGL5 inks could be easily squeezed out from the nozzle at room temperature and could immediately return to high viscosity after being squeezed out of the nozzle. Immediately after printing, the scaffold was irradiated with 365 nm UV light to initiate polymerization. As shown in **Figure 7B and C**, the bracket could be folded at will to withstand various deformations without damage. Further sweep frequency and stress amplitude sweep test were carried out on NGL3 and NGL5 (**Figure 7D-F**). Obviously, in the tested frequency range, the G' values of all the samples were

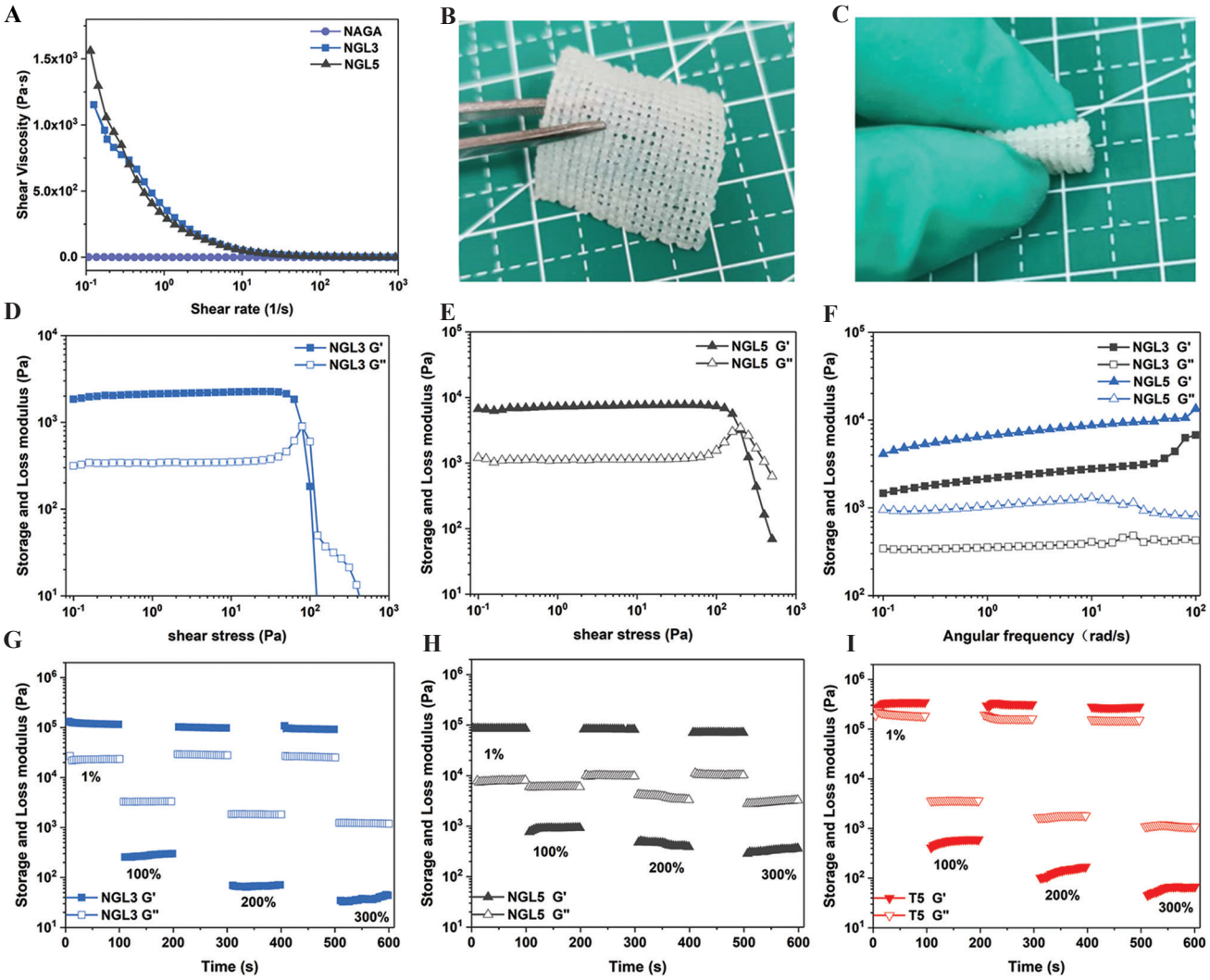

Figure 7. Rheological properties of samples. (A) Shear viscosity-shear rates of the various hydrogels. (B And C) Macroscopic observations of 3D-printed NGL3 hydrogel constructs. Results of stress amplitude sweep tests (D) NGL3 and (E) NGL5. (F) The G' and G" values of the NGL3 and NGL5 hydrogels. The variation in the G' and G" values of (G) NGL3, (H) NGL5, and (I) T5 hydrogel when switching the alternate step strain from minor strain (1%) to enormous strain (100%, 200%, and 300%) at a fixed frequency of 1 Hz and temperature of 25°C.

higher than the G" values, indicating that the ink exhibited a "gel-like" behavior and stable mechanical properties. The self-supporting ability could achieve high-fidelity printing of the scaffold[39].

As shown in **Figure 7G-I**, at a low shear strain (1%) at 25°C, the G' and G" remained almost unchanged, where the former value was greater than that of the latter. This indicated that the hydrogel network presented gel-like elastic properties under a minor strain. The amplitude oscillatory strains were switched from minor strain (100 s for each interval) to large strain (100%, 200%, or 300%, 100 s for each interval), the G" was more significant than the G', implying that the viscous behavior dominated the hydrogel network[40]. When the shear strain dropped to 1%, the G' quickly returned to its initial value, which indicated that once the enormous strain was removed, the hydrogel realized the reconstruction of the network structure due to the reformation of the hydrogen bonds. This showed the recovery ability of the hydrogel after a continuous large deformation. **Figure 7I** and **Figure S2** indicate that the G' of the TA-treated hydrogel gradually increased and was higher than the untreated hydrogel. Because TA provided reversible hydrogen bonds, the movement of polymer chains in the T5 sample was confined to relaxation at enormous strain. Therefore, T5 hydrogel exhibited a higher G' values[41]. The mechanical and rheological analyses proved that TA improved the mechanical properties.

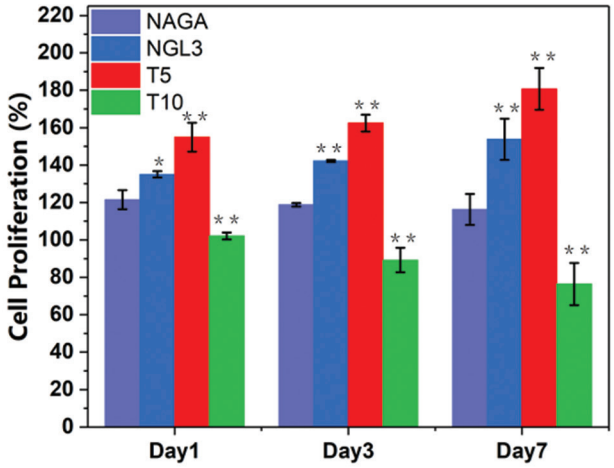

Figure 8. Cell proliferation of BMSCs cultured on NAGA, NGL3, T5, and T10 hydrogels.

3.6. Biocompatibility and osteochondral activity

The NAGA, NGL3, and T5 hydrogels showed good biocompatibility (**Figure 8**). Compared with NAGA, the addition of clay and GelMA increased cell proliferation. It is worth noting that with the addition of TA, the cell proliferation on the T5 hydrogel increased significantly on the 7th day. The enhanced cell activity could be attributed

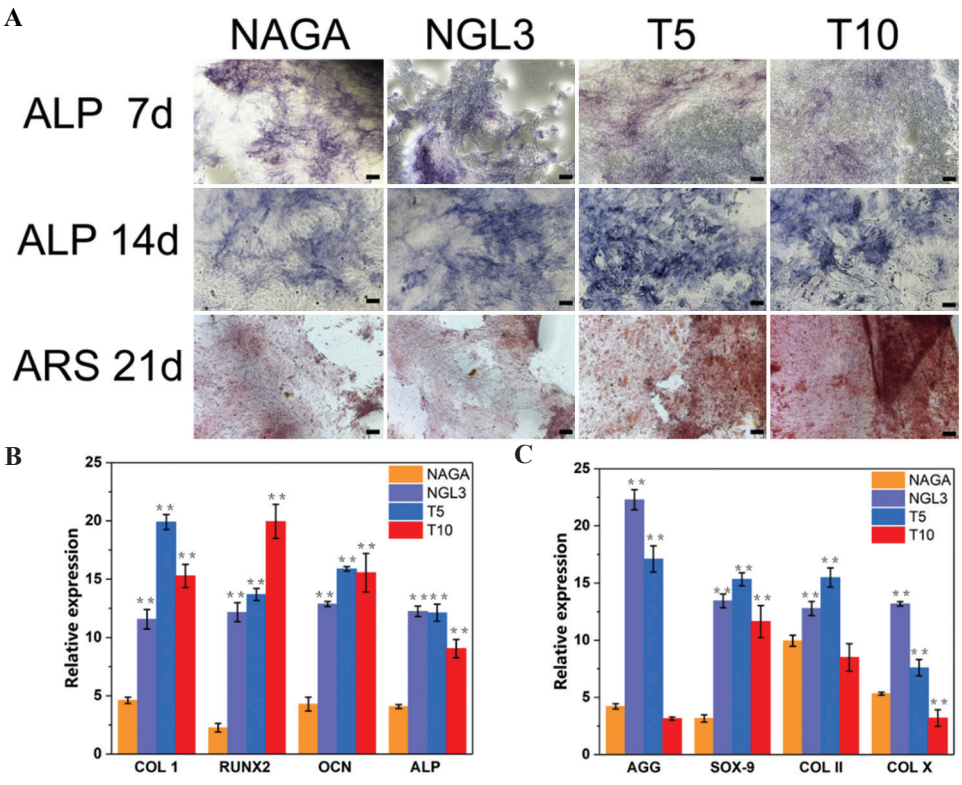

Figure 9. (A) Alkaline phosphatase activity assay and calcium deposition assay. Osteogenic (B) and chondrogenic (C) gene expression of BMSCs cultured on a NAGA, NGL3, T5, and T10 hydrogel (scale bar: 100 μm).

to reduced swelling and a more significant number of interaction sites for cell attachment[42]. However, for the T10 hydrogel, the growth rate of the BMSCs was slow. This might have occurred because the excessive crosslinking density was not conducive to cell growth[15]. In this study, the T5-mediated hydrogel promoted the significant proliferation of BMSCs.

To study the osteogenic differentiation of the hydrogels, the ALP and ARS activities and expression of osteogenic genes were evaluated. As shown in **Figure 9A**, the expression of ALP increased with culture time. Among them, the T5 group had the highest expression of ALP, and the NAGA group had the lowest expression. The ARS results revealed more mineralized nodules in the T5 and T10 groups, and the staining of the mineralized matrix was significantly deepened. The osteogenic gene expression (COL I, RUNX2, OCN, and ALP) of BMSCs in the NGL3, T5, and T10 hydrogels was considerably higher than that in the NAGA hydrogels (**Figure 9B**). This showed that adding clay and TA to the hydrogel could synergistically promote the osteogenic differentiation of BMSCs. Nanoclay has been associated with enhanced osteogenic differentiation. The previous research confirmed that TA has excellent antioxidant activity, quenches the over-expressed ROS of cells, protects stem cells from oxidative stress damage, and promotes osteogenic differentiation[43]. In summary, these results proved that the T5 hydrogel had excellent osteogenic properties and could promote the osteogenic differentiation of BMSCs (**Figure S3**).

Furthermore, the chondrogenic differentiation of the hydrogels was studied and the expression of chondrogenic genes was evaluated. The expression of AGG, SOX9, and COLII genes in the NGL3 and T5 hydrogels was significantly higher than in the NAGA and T10 hydrogels (**Figure 9C**). The lower expression of COLX in T5 and T10 hydrogels indicated that tannins could prevent cells from differentiating into a hypertrophic phenotype. The AGG gene expression of the BMSCs in the NGL3 group was approximately 5 times higher than that of the cells in the NAGA group. In terms of chondrogenic gene expression of AGG, COLII, and SOX9 genes, the expression of the T10 hydrogel was significantly lower than that of T5, indicating that when the TA concentration reached 10%, it was not conducive to the expression of chondrogenic genes.

4. Conclusion

A novel multifunctional hydrogel was developed using a two-step method. The interaction of multiple hydrogen bonds between the TA and NAGA/GelMA could dissipate energy and improve the hydrogel's mechanical strength and fatigue resistance. The swelling rates of the hydrogels were significantly reduced. The TA gave the hydrogel significant oxidation resistance and adhesion. The TA-mediated composite hydrogel promoted the significant proliferation of BMSCs and osteogenic and chondrogenic differentiation. The developed multifunctional composite hydrogel could be a promising candidate for osteochondral defect repair in the treatment of osteoarthritis.

Acknowledgments

This work was supported by the National Natural Science Foundation of China (Grant No.52075324) and the Cross-Institute Research Fund of Shanghai Jiao Tong University (Grant No. YG2021ZD06).

Conflict of interest

The authors declare no conflict of interest.

Author contributions

All authors have made substantial contributions to conception and design of the study. X. Li guided and supervised the project. L.L. Dong and Z.Z. Han conducted experiments and contributed intellectually to the scientific design of the project.

References

1. Fang B, Qiu P, Xia C, *et al.*, 2021, Extracellular Matrix Scaffold Crosslinked with Vancomycin for Multifunctional Antibacterial Bone Infection Therapy. *Biomaterials*, 268:120603. https://doi.org/10.1016/j.biomaterials.2020.120603
2. Tao B, Lin C, Yuan Z, *et al.*, 2021, Near Infrared Light-triggered On-demand Cur Release from Gel-PDA@Cur Composite Hydrogel for Antibacterial Wound Healing. *Chem Eng J*, 403:126182. https://doi.org/10.1016/j.cej.2020.126182
3. Wang Y, Ma M, Zhang L, *et al.*, 2019, Fabrication of Bi-layer Photocrosslinked GelMA/PEGDA Fibrous Membrane for Guided Bone Regeneration Materials. *Mater Lett*, 249:112–5. https://doi.org/10.1016/j.matlet.2019.04.076
4. Ahmadian Z, Correia A, Hasany M, *et al.*, 2021, A Hydrogen-bonded Extracellular Matrix-mimicking Bactericidal Hydrogel with Radical Scavenging and Hemostatic Function for pH-Responsive Wound Healing Acceleration. *Adv Healthc Mater*, 10:2001122. https://doi.org/10.1002/adhm.202001122
5. Walker BW, Lara RP, Yu CH, *et al.*, 2019, Engineering a Naturally-derived Adhesive and Conductive Cardiopatch. *Biomaterials*, 207:89–101. https://doi.org/10.1016/j.biomaterials.2019.03.015
6. Zhou F, Hong Y, Zhang X, *et al.*, 2018, Tough Hydrogel with Enhanced Tissue Integration and *in Situ* Forming Capability for Osteochondral Defect Repair. *Appl Mater Today*, 13:32–44.

https://doi.org/10.1016/j.apmt.2018.08.005

7. Heinrich MA, Liu W, Jimenez A, *et al.*, 2019, 3D Bioprinting: From Benches to Translational Applications. *Small*, 15:1805510. https://doi.org/10.1002/smll.201805510
8. Haq M A, Su Y, Wang D, 2017, Mechanical Properties of PNIPAM Based Hydrogels: A Review. *Mater Sci Eng C*, 70:842–55. https://doi.org/10.1016/j.msec.2016.09.081
9. Mousa M, Evans ND, Oreffo R O C, *et al.*, 2018, Clay nanoparticles for regenerative medicine and biomaterial design: A review of clay bioactivity. *Biomaterials*, 159:204–14. https://doi.org/10.1016/j.biomaterials.2017.12.024
10. Wei Y, Xiang L, Ou H, *et al.*, 2020, MXene-based Conductive Organohydrogels with Long-term Environmental Stability and Multifunctionality. *Adv Funct Mater*, 30:2005135. https://doi.org/10.1002/adfm.202005135
11. Ye Y, Zhang Y, Chen Y, *et al*., 2020, Cellulose Nanofibrils Enhanced, Strong, Stretchable, Freezing-tolerant Ionic Conductive Organohydrogel for Multi-Functional Sensors. *Adv Funct Mater*, 30:2003430. https://doi.org/10.1002/adfm.202003430
12. Hong S, Sycks D, Chan HF, *et al.*, 2015, 3D Printing of Highly Stretchable and Tough Hydrogels into Complex, Cellularized Structures. *Adv Mater*, 27:4035–40. https://doi.org/10.1002/adma.201501099
13. Maiti C, Imani KB, Yoon J, 2021, Recent Advances in Design Strategies for Tough and Stretchable Hydrogels. *ChemPlusChem*, 86:601–11. https://doi.org/10.1002/cplu.202100074
14. Chen Y, Qiu Y, Wang Q, *et al.*, 2020, Mussel-inspired Sandwich-like Nanofibers/Hydrogel Composite with Super Adhesive, Sustained Drug Release and Anti-infection Capacity. *Chem Eng J*, 399:125668. https://doi.org/10.1016/j.cej.2020.125668
15. Zhai X, Ma Y, Hou C, *et al.*, 2017, 3D-Printed High Strength Bioactive Supramolecular Polymer/Clay Nanocomposite Hydrogel Scaffold for Bone Regeneration. *ACS Biomater Sci Eng*, 3:1109–18. https://doi.org/10.1021/acsbiomaterials.7b00224
16. Liu X, Yang Y, Niu X, *et al.*, 2017, An *in Situ* Photocrosslinkable Platelet Rich Plasma-complexed Hydrogel Glue with Growth Factor Controlled Release Ability to Promote Cartilage Defect Repair. *Acta Biomater*, 62:179–87. https://doi.org/10.1016/j.actbio.2017.05.023
17. Yu Y, Shen X, Luo Z, *et al.*, 2018, Osteogenesis Potential of Different Titania Nanotubes in Oxidative Stress Microenvironment. *Biomaterials*, 167:44–57. https://doi.org/10.1016/j.biomaterials.2018.03.024
18. Atashi F, Modarressi A, Pepper MS, 2015, The Role of Reactive Oxygen Species in Mesenchymal Stem Cell Adipogenic and Osteogenic Differentiation: A Review. *Stem Cells Dev*, 24:1150–63. https://doi.org/10.1089/scd.2014.0484
19. Jiao H, Xiao E, Graves DT, 2015, Diabetes and Its Effect on Bone and Fracture Healing. *Curr Osteop Reports*, 13:327–35. https://doi.org/10.1007/s11914-015-0286-8
20. Nadgorny M, Collins J, Xiao Z, *et al.*, 2018, 3D-printing of Dynamic Self-healing Cryogels with Tuneable Properties. *Polymer Chem*, 9:1684–92. https://doi.org/10.1039/C7PY01945A
21. Zhou L, Ramezani H, Sun M, *et al.*, 2020, 3D Printing of High-strength Chitosan Hydrogel Scaffolds without any Organic Solvents. *Biomater Sci*, 8:5020–8. https://doi.org/10.1039/d0bm00896f
22. Ge W, Cao S, Shen F, *et al.*, 2019, Rapid Self-healing, Stretchable, Moldable, Antioxidant and Antibacterial Tannic Acid-cellulose Nanofibril Composite Hydrogels. *Carbohydrate Polymers*, 224:115147. https://doi.org/10.1016/j.carbpol.2019.115147
23. Lin F, Wang Z, Shen Y, *et al.*, 2019, Natural Skin-inspired Versatile Cellulose Biomimetic Hydrogels. *J Mater Chem A*, 7:26442–55. https://doi.org/10.1039/C9TA10502F
24. Li Q, Xu S, Feng Q, *et al.*, 2021, 3D Printed Silk-gelatin Hydrogel Scaffold with Different Porous Structure and Cell Seeding Strategy for Cartilage Regeneration. *Bioactive Mater*, 6:3396–410. https://doi.org/10.1016/j.bioactmat.2021.03.013
25. Osi AR, Zhang H, Chen J, *et al.*, 2021, Three-Dimensional-Printable Thermo/Photo-Cross-Linked Methacrylated Chitosan-Gelatin Hydrogel Composites for Tissue Engineering. *ACS Appl Mater Interfaces*, 13:22902–13. https://doi.org/10.1021/acsami.1c01321
26. Shirahama H, Lee BH, Tan LP, *et al.*, 2016, Precise Tuning of Facile One-Pot Gelatin Methacryloyl (GelMA) Synthesis. *Sci Reports*, 6:11. https://doi.org/10.1038/srep31036
27. Dong L, Bu Z, Xiong Y, *et al.*, 2021, Facile Extrusion 3D Printing of Gelatine Methacrylate/Laponite Nanocomposite Hydrogel with High Concentration Nanoclay for Bone Tissue Regeneration. *Int J Biol Macsromol*, 188:72–81. https://doi.org/10.1016/j.ijbiomac.2021.07.199

28. Kim BJ, Oh DX, Kim S, *et al.*, 2014, Mussel-Mimetic Protein-Based Adhesive Hydrogel. *Biomacromolecules*, 15:1579–85. https://doi.org/10.1021/bm4017308
29. Hong KH, 2017, Polyvinyl Alcohol/tannic Acid Hydrogel Prepared by a Freeze-thawing Process for Wound Dressing Applications. *Polymer Bull*, 74:2861–72. https://doi.org/10.1007/s00289-016-1868-z
30. He X, Liu X, Yang J, *et al.*, 2020, Tannic Acid-reinforced Methacrylated Chitosan/Methacrylated Silk Fibroin Hydrogels with Multifunctionality for Accelerating Wound Healing. *Carbohydrate Polymers*, 247:116689. https://doi.org/10.1016/j.carbpol.2020.116689
31. Jin Y, Liu C, Chai W, *et al.*, 2017, Self-Supporting Nanoclay as Internal Scaffold Material for Direct Printing of Soft Hydrogel Composite Structures in Air. *ACS Appl Mater Interfaces*, 9:17456–65. https://doi.org/10.1021/acsami.7b03613
32. Liang Q, Gao F, Zeng Z, *et al.*, 2020, Coaxial Scale-Up Printing of Diameter-Tunable Biohybrid Hydrogel Microtubes with High Strength, Perfusability, and Endothelialization. *Adv Funct Mater*, 30:2001485. https://doi.org/10.1002/adfm.202001485
33. Fan Y, Zhou G, Zhang G, *et al.*, 2020, Comparative Study on the Mechanical Behavior of the Interface between Natural Cartilage and Artificial Cartilage. *Soft Mater*, 19:1–20. https://doi.org/10.1080/1539445X.2020.1851258
34. Gaharwar AK, Rivera CP, Wu CJ, *et al.*, 2011, Transparent, Elastomeric and Tough Hydrogels from Poly(ethylene Glycol) and Silicate Nanoparticles. *Acta Biomater*, 7:4139–48. https://doi.org/10.1016/j.actbio.2011.07.023
35. Kong HJ, Wong E, Mooney DJ, 2003, Independent Control of Rigidity and Toughness of Polymeric Hydrogels. *Macromolecules*, 36:4582–8. https://doi.org/10.1021/ma034137w
36. Chen YC, Lin RZ, Qi H, *et al.*, 2012, Functional Human Vascular Network Generated in Photocrosslinkable Gelatin Methacrylate Hydrogels. *Adv Funct Mater*, 22:2027–39. https://doi.org/10.1002/adfm.201101662
37. Cui C, Fan C, Wu Y, *et al.*, 2019, Water-Triggered Hyperbranched Polymer Universal Adhesives: From Strong Underwater Adhesion to Rapid Sealing Hemostasis. *Adv Mater*, 31:1905761. https://doi.org/10.1002/adma.201905761
38. Li X, 2017, 2-Phenyl-4,4,5,5-tetramethylimidazoline-1-oxyl 3-Oxide (PTIO) Radical Scavenging: A New and Simple Antioxidant Assay *In Vitro*. *J Agric Food Chem*, 65:6288–97. https://doi.org/10.1021/acs.jafc.7b02247
39. Nadgorny M, Collins J, Xiao Z, *et al.*, 2017, 3D-printing of Dynamic Self-healing Cryogels with Tuneable Properties. *Polymer Chem*, 9:01945. https://doi.org/9. 10.1039/C7PY01945A
40. Zhang Y, Yang B, Zhang X, *et al.*, 2012, A Magnetic Self-healing Hydrogel. *Chem Commun*, 48:9305–7. https://doi.org/10.1039/C2CC34745H
41. Deng G, Li F, Yu H, *et al.*, 2012, Dynamic Hydrogels with an Environmental Adaptive Self-Healing Ability and Dual Responsive Sol-Gel Transitions. *ACS Macro Lett*, 1:275–9. https://doi.org/10.1021/mz200195n
42. Discher D, Janmey P, Wang YL, 2005, Tissue Cells Feel and Respond to the Stiffness of Their Substrate. *Science*, 310:1139–43. https://doi.org/10.1126/science.1116995
43. Yang J, Liang J, Zhu Y, *et al.*, 2021, Fullerol-hydrogel Microfluidic Spheres for *In Situ* Redox Regulation of Stem Cell Fate and Refractory Bone Healing. *Bioactive Mater*, 6:4801–15. https://doi.org/10.1016/j.bioactmat.2021.05.024

Publisher's note